sciendo
Power Electronics and Drives
Volume 9(44), 2024 DOI: 10.2478/pead-2024-0027

A Novel Method to Obtain Reverse Bias I–V Curves for Single Cells Integrated in Photovoltaic Modules

Research paper

Mahmoud Drif*, Ahmed Bouchelaghem, Abderezak Guemache, Djoubair Abdelouahab Benhamadouche, Djamel Saigaa

Department of Electronics, Faculty of Technology, University of M'sila, 28000 M'sila, Algeria

Received: 27 April 2024; Accepted: 25 June 2024

Abstract: Despite the existence of accurate mathematical models facilitating the analysis of photovoltaic (PV) sources' behaviour under diverse conditions, including normal operation and situations involving mismatch phenomena such as partial shadowing and various faults (i.e., PV cells operating in forward bias and reverse bias quadrants), an important issue still persists. Crucial parameters essential for adjusting these models, particularly those related to reverse-biased characteristics such as breakdown voltage, are often absent in manufacturers' datasheets. This omission presents a substantial challenge, as it restricts the ability to acquire comprehensive and accurate information required for a thorough analysis of devices in the second quadrant. To address this issue, our research introduces a novel method for measuring the reverse-biased I–V characteristics of individual PV cells within a module without having to dissociate them from the PV module encapsulants. The process involves measuring the forward-bias I–V curves of both the fully illuminated PV module and a partially shaded PV module with only one completely shaded cell. This can be achieved outdoors and by utilising commercially available I–V tracers. Thus, the reverse I–V curve can easily be derived from these forward bias I–V curves. Finally, the proposed method serves as a nondestructive technique for characterising solar cells in the second quadrant. This innovative approach offers a promising solution for assessing the performance and health of PV modules without causing damage and may result in significant cost savings.

Keywords: *forward bias I–V curve • reverse bias I–V curve • forward parameters • reverse parameters • roger model • bishop model • Quashning model*

1. Introduction

Photovoltaic (PV) cells are commonly connected in series within a PV module to safeguard them from damage and achieve the necessary voltage. This is necessary as the voltage output of a single PV cell is usually insufficient on its own. By connecting multiple cells in series, the voltage can be raised to a level suitable for various applications. Moreover, wiring cells in series aids in protecting individual cells from potential harm caused by abnormal operating conditions, such as overloading and overheating (Aktaş and Kirçiçek, 2021; Nehme et al., 2021).

The current–voltage (I–V) characteristic of a PV cell resembles that of a Shockley diode, which can operate in three quadrants of the I–V curve plotted on a Cartesian plane, as shown in Figure 1 (Häberlin, 2012). These quadrants are follows: The first quadrant (QI) or forward bias, where the current flows from the anode to the cathode ($V > 0$ and $I > 0$). This is the normal operating mode for a PV cell, where energy is generated. The second quadrant (QII) or reverse bias region, where the current flows from the cathode to the anode ($V < 0$ and $I > 0$). This mode is not normally used for PV cells, but it can occur if the cell is reverse biased and absorbs energy rather than outputting it. The third quadrant (QIII), which represents the reverse direction of the PV cell, is generally not relevant for its normal operation. The fourth quadrant (QIV) or breakdown, where the current increases rapidly with a small

* *Email: mahmoud.drif@univ-msila.dz*

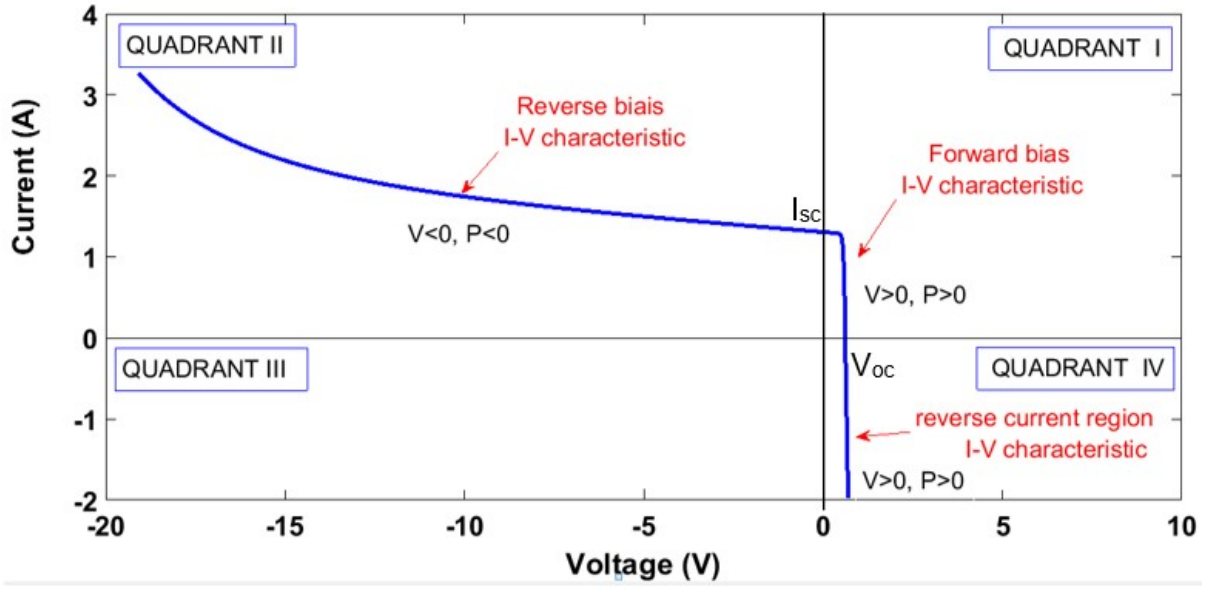

Figure 1. Forward and reverse bias I–V characteristics of a PV cell showing all the working regions. PV, photovoltaic.

increase in voltage. This mode is not normally used for PV cells, but it can occur if the cell is reverse biased too strongly.

The forward bias I–V characteristic curve is essentially a graphical representation in the first power quadrant (QI) illustrating the operation of any PV device, such as a PV cell or module, as a DC generator. It summarises the correlation between the output current and output voltage at a given solar irradiance and temperature. It extends from the short-circuit current (Isc) to the open-circuit voltage (Voc), which for crystalline PV cells is typically around 0.6V. Reference I–V curves, determined for specified operating conditions (standard test conditions [STC]: 1,000W/m², 25°C, solar spectrum AM1.5), are typically provided by manufacturers. In general, the forward bias I–V characteristic curve is a valuable tool for understanding the performance of PV devices. It can be used to identify a PV device, to determine its key performance parameters, such as the open-circuit voltage (V_{oc}), the short-circuit current (I_{sc}), and the current and voltage at the maximum power point (V_m, I_m), and to optimise its operation.

Regarding the second quadrant (QII), reverse-bias characteristics are often ignored since PV cells are not designed to operate in the reverse-biased region, and doing so can damage the cell (Kim et al., 2013). However, if any malfunction occurs, such as during shading, a PV cell will not be able to generate electricity. Instead, it can still be operated in the second quadrant that has a much more extensive characteristic limited by the breakdown voltage (V_{br}). This is because the shaded cell can potentially reverse its polarity and act as a load, consuming the energy generated by the other cells in the module. In addition, for a high voltage whose value is around the avalanche zone of a cell, it can carry a current that exceeds its short-circuit current and can theoretically reach an infinite value. This can lead to the shaded cell heating up and eventually being destroyed. This phenomenon is called the hot spot effect. Therefore, it is important to consider reverse-bias characteristics when designing and operating PV systems.PV devices are typically modelled based on their forward-biased characteristics. The most common classic models include the single-diode model (SDM) and the double-diode model (DDM), which are fully detailed in the next section. In these models, all unknown parameters can be extracted from the manufacturer's datasheet or measured data. However, these classic models are not conclusive for handling cell shading issues and various other faults. Specifically, they lack reverse-bias characteristics. Solar cell vendors typically do not provide manufacturing and technical material data regarding solar cell operation in the second power quadrant, making such information unavailable to the public (Petrone et al., 2017). Hence, to fully examine PV cell behaviour under normal environmental conditions, including mismatch phenomena and various faults, it is necessary to analyse the complete characteristic curves of actual PV cells, extending from V_{oc} to the breakdown voltage V_{br}. Consequently, classic models had to be extended to encompass the negative section of the PV cell characteristics. In this context, several more detailed PV models have been proposed and are described in the literature (Petrone et al., 2017).

Unfortunately, essential parameters required to adjust PV cell models, particularly those pertaining to reverse-bias characteristics like breakdown voltage, are not provided in the manufacturers' datasheets. This omission presents a substantial challenge, as it restricts the ability to acquire comprehensive and accurate information required for a thorough analysis of devices behaviour in the second quadrant (QII). Consequently, limitations in understanding reverse-bias characteristics can lead to inaccurate performance predictions and suboptimal design of PV systems, especially under real-world conditions involving partial shading or another mismatch (Hurkx, 1992; Subramanian and Darling, 2001).

To address this issue, our research introduces a simple and an indirect method for measuring the reverse I–V characteristics of individual PV cells as part of PV module without the need to dissociate them from the PV module encapsulants. This is can be achieved by utilising commercially available I–V tracers. The process involves measuring outdoor the I–V curve of a fully illuminated PV module and the I–V curve of a module with only one fully shaded cell (PV cell in dark). From these curves, the reverse I–V curve might be obtained. This technique offers a convenient and nondestructive method for reverse-bias measurement of individual PV cells within a module while maintaining the integrity of the encapsulation and promises cost savings.

This paper is organised as follows: Section 2 provides insight into the available mathematical models describing the behaviour of PV cells in the first quadrant, along with their implicit and explicit forms. Section 3 is devoted to the models commonly used to describe the behaviour of cells operating in the second quadrant, as well as their relevant parameters. In Section 4, the basic concept and principle of the proposed method for measuring the reverse bias I–V curve are proposed. Finally, the experimental validation and discussion of the results obtained will be presented in Section 5.

2. Classic Models of PV Cells

As aforementioned, there are two classic models commonly employed to describe the behaviour of direct current in the forward bias region (or first quadrant: QI). These models are the SDM and the DDM.

The SDM, also known as a five-parameter model, is the most widespread model used for PV cells and PV modules due to its low complexity and good accuracy in the power-generating quadrant (QI). Due to its simplicity in use on one hand and often acceptable accuracy on the other hand, the SDM has been widely used to study the behaviour of PV sources under various weather conditions, including both uniform irradiance and nonuniform distributions, such as partial shading (Bastidas et al., 2013; Drif et al., 2021; Gallardo-Saavedra and Karlsson, 2018; Kadri et al., 2012; Karatepe et al., 2007; Patel and Agarwal, 2008; Petrone and Ramos, 2011; Petrone et al., 2007; Ramabadran, 2009; Samer et al., 2012; Villalva et al., 2009; Wang and Hsu, 2009; Wei et al., 2012).

Similarly, the DDM, also known as the seven-parameters model, offers a good compromise between complexity and accuracy. Using this model, higher precision can be achieved. In this regard, several research works have been reported in the literature, focusing on calculating the current–voltage characteristic and the output power of a PV generator at different levels of granularity and in the presence of shading phenomena, among others (Babu et al., 2015; Duong et al., 2017; Gbadega Peter and Saha, 2019; Ishaque and Salam, 2013; Ishaque et al., 2011; Kermadi et al., 2020; Kreft et al., 2021; Moreira et al., 2021; Paraskevadaki et al., 2011; Rathee, 2013; Varshney et al., 2016; Yin and Babu, 2018).

In the following sections, we will present the mathematical expressions governing SDM and DDM models in both their implicit and explicit forms.

2.1. Implicit form I = f (V, I)

According to their electrical equivalent circuits depicted previously in Figures 2a and 2b, the SDM and DDM are well known as the single exponential model and the double exponential model, respectively. Their expressions can be summarised by the implicit function given in Eq. (1). To use the single exponential model, set (i = 1), and to use the double exponential model, set (i = 2).

$$I = I_{ph} - \left(\sum_{i=1}^{i=2} I_{oi} \left[\exp\left(q \frac{V + R_s I}{A_i k T} \right) - 1 \right] \right) - \frac{V + R_s I}{R_{sh}} \tag{1}$$

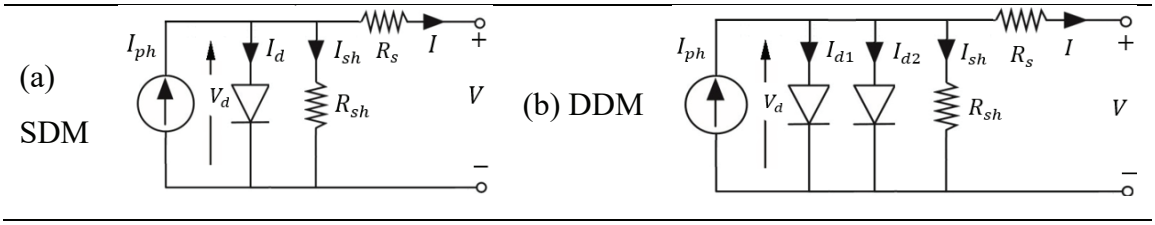

Figure 2. Classic equivalent-circuits models of a PV cell. a) Single Diode Model (SDM), b) Double Diode Model (DDM).

In this equation $I_{ph}, R_s, R_{sh}, I_{oi}$, and A_i are the parameters of the model that are related to the internal properties of the PV cell. They denote, respectively, the light-generated current (or photocurrent), the series resistance, the shunt resistance, the reverse saturation current of diode, and the ideality factor. The rest of the known parameters are the Boltzmann constant (k = 1.3806503 × 10^{-23} J/K), the electron charge (q = 1.60217646 × 10^{-19} C), and the temperature of junction in Kelvin. It is worth noting that the SDM contains five undetermined parameters, namely, $I_{ph}, R_s, R_{sh}, I_{oi}$, and *A*, while the DDM includes seven undetermined parameters, i.e., $I_{ph}, R_s, R_{sh}, I_{oi}$, A_1 and A_2. To further simplify the DDM, several researchers have considered that $(A_1 = 1)$ and $(A_2 = 2)$, which leads to a decrease in the number of parameters to 5.

2.2. Explicit forms I = f (V) and V = g(I)

Due to the transcendental and implicit nature of the I–V equations describing the classic models (SDM and DDM), another modelling method directly addresses the problem of solving the transcendental I–V equation in a quite original way. Instead of using numerical approximation, this method employs a rather special mathematical function called the Lambert W function (or simply the W function). By employing this approach, we circumvent the need to solve the transcendental I–V equations directly. This is achieved by analytically solving their explicit forms, which express the current as a function of voltage $\left(I = f\left(V\right)\right)$ and its inverse $(V = g(I))$. To reduce the complexity of the SDM and DDM models (as shown in Eq. (1)), approximations are introduced, leading to the simplified equations presented in Eqs. (2)–(5) (Batzelis et al., 2014; Batzelis et al., 2020; Ćalasan et al., 2020; Jain and Kapoor, 2004; Jain et al., 2006; Lun et al., 2015; Ortiz-Conde and Sánchez, 2005; Peng et al., 2013; Petrone et al., 2007; Picault et al., 2010; Roibás-millán et al., 2020; Tripathy et al., 2017).

The SDM, in its explicit form, is given by Eqs. (2) and (3), which express the current as a function of voltage $\left(I = f\left(V\right)\right)$ or the voltage as a function of current $V = g\left(I\right)$ as follows:

$$I = f\left(V\right) = \frac{R_{sh}\left(I_{ph} + I_o\right) - V}{R_s + R_{sh}} - \frac{1}{R_s}\frac{AkT}{q}W\left\{q\frac{R_s R_{sh} I_o}{AkT\left(R_s + R_{sh}\right)}\exp\left[q\frac{R_{sh}\left(R_s I_{ph} + R_s I_o + V\right)}{AkT\left(R_s + R_{sh}\right)}\right]\right\} \tag{2}$$

$$V = g\left(I\right) = R_{sh}\left(I_{ph} + I_o\right) - \left(R_s + R_{sh}\right)I - A\frac{kT}{q}.\,W\left\{q\frac{R_{sh} I_o}{AkT}\exp\left[q\frac{R_{sh}\left(I_{ph} + I_o - I\right)}{A\,kT}\right]\right\} \tag{3}$$

Regarding the DDM in its explicit form, it is represented by Eqs. (4) and (5) $\left(I = f\left(V\right)\right)$ or $\left(V = g\left(I\right)\right)$ as follows:

$$I = f\left(V\right) = \frac{R_{sh}\left(I_{ph} + I_{o1} + I_{o2}\right) - V}{R_s + R_{sh}} - \frac{1}{2R_s}\frac{kT}{q}\sum_{i=1}^{2}A_i W\left\{q\frac{R_s R_{sh}\left(I_{o1} + I_{o2}\right)}{A_i kT\left(R_s + R_{sh}\right)}\exp\left[q\frac{R_{sh}\left(R_s I_{ph} + R_s I_{o1} + R_s I_{o2} + V\right)}{A_i kT\left(R_s + R_{sh}\right)}\right]\right\} \tag{4}$$

$$V = g\left(I\right) = R_{sh}\left(I_{ph} + I_{o1} + I_{o2} - I\right) - R_s I - \frac{1}{2}\frac{kT}{q}\sum_{i=1}^{2}A_i W\left\{q\left[\exp\frac{R_{sh}\left(I_{ph} + I_{o1} + I_{o2} - I\right)}{A_i kT}\right]\right\} \tag{5}$$

Where $I_{ph}, R_s, R_{sh}, I_{oi}$ and A_i (for $i = 1,2$) have their conventional meanings.

3. Extended Models of PV Cells

As previously mentioned, the classic models are established to describe only the I–V characteristic in the first quadrant, which makes them insufficient to handle problems such as shade on cells, hotspot, etc. To address this limitation, some scholars developed and enhanced the SDM and the DDM models by introducing an extension term that describes the behaviour in the second quadrant, i.e., at reverse-bias voltages. In this context, several equations have been proposed in the literature to simulate the behaviour of PV cells in both the forward- and reverse-bias regions. Many of these equations stem from the conventional I–V equation in the forward region, modified to introduce avalanche effects. The main contributions, presented in chronological order, are summarised in the following sections.

3.1. Model of Roger

To analyse the mismatch effect that occurs in PV cells under abnormal conditions like cell damage or partial shading, Roger and Maguin (1982) proposed a piecewise model. This model is defined by two subfunctions (Eq. (6)) that describe the I–V behaviour in different voltage regions. The first subfunction is a simplified version of the SDM that neglects the shunt resistance effect. It is used to describe the forward bias region (positive voltage) where $V \succ R_s I$. The second subfunction is an empirical equation defined as a quadratic function of the applied voltage. This equation accounts for the cell's behaviour under reverse bias (negative voltage) where $V < -R_s I$.

$$I = \begin{cases} I_{ph} - I_o \left[\exp\left(q \dfrac{V - R_s I}{A\, kT} \right) - 1 \right] & if\ V > -R_s\ I \\ I = I_{ph} + B_{rev} \left(V + R_s I \right)^2 & if\ V < -R_s\ I \end{cases} \tag{6}$$

Where $I_{ph}, R_s, R_{sh}, I_{oi}$, and *A* have their conventional meanings and B_{rev} is a fitting coefficient.

3.2. Model Bishop

To analyse the behaviour of the PV cell in two quadrants, Bishop (1988) proposes an equation in which the avalanche breakdown is expressed as a nonlinear multiplication factor that affects the shunt resistance term in the SDM. The additional term introduced by Bishop reproduces the high current in the cell during avalanche breakdown at high negative voltages. From an electrical point of view, the branch of the cell equivalent circuit containing the shunt resistance is completed with a voltage-controlled current source, as shown in Figure 3. Consequently, the complete equation becomes:

$$I = I_{ph} - I_o \left[\exp\left(q \frac{V + R_s I}{A\, kT} \right) - 1 \right] - \frac{V + R_s I}{R_{sh}} - \underbrace{a \left(\frac{V + R_s I}{R_{sh}} \right) \left(1 - \frac{V + R_s I}{V_{br}} \right)^{-n}}_{\text{Extension term}} \tag{7}$$

Where I_{ph}, R_s, R_{sh}, I_o, and *A* have their conventional meanings, V_{br} is the junction breakdown voltage, ***a*** is the fraction of ohmic current involved in avalanche breakdown, and ***n*** the avalanche breakdown exponent.

In this model, eight parameters should be estimated to reproduce the behaviour of a PV cell using the Bishop model: $I_{ph}, R_s, R_{sh}, I_o, A, V_{br}, a$ and ***n***.

3.3. Model of Quashning

Quashaning (Quashning and Hanitsch, 1996) followed Bishop's approach by incorporating the same extension term to the DDM model, which accounts for diode breakdown at high negative voltages. The branch of the cell equivalent circuit is completed with a voltage-controlled current generator in parallel with the shunt resistance, as shown in Figure 4. The representation of this model is provided in Figure 4. Consequently, the PV cell current can be expressed as follows:

$$I = I_{ph} - \left(\sum_{i=1}^{2} I_{oi} \left[\exp\left(q \frac{V + R_s I}{A_i kT} \right) - 1 \right] \right) - \frac{V + R_s I}{R_{sh}} - \underbrace{a \left(V + R_s I \right) \left(1 - \frac{V + R_s I}{V_{br}} \right)^{-n}}_{\text{Extension term}} \tag{8}$$

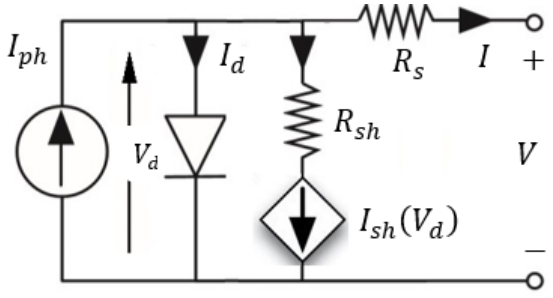

Figure 3. Equivalent-circuit of Bishop's model.

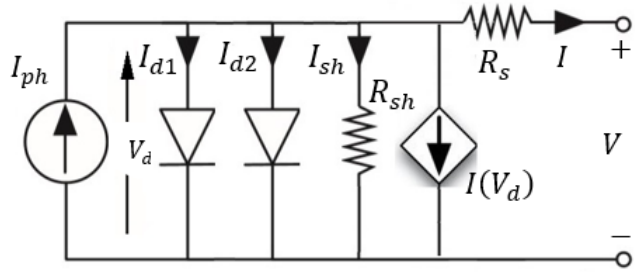

Figure 4. Equivalent-circuits of Quashning's model.

In this model, ten parameters should be estimated to reproduce the behaviour of a PV cell using the Quashning model: $I_{ph}, R_s, R_{sh}, I_{o1}, I_{o2}, A_1, A_2, V_{br}, a$, and n.

4. Proposed Method for Measuring the Reverse-Bias Characteristic of a PV Cell

4.1. Basic concept of the proposed method

In a series connection of PV cells, as is the case with a PV module, if a single cell is exposed to shade, regardless of the amount, the module's maximum power output is significantly reduced and its characteristic curves are altered. This effect is depicted in Figure 5. In such a case, the short-circuit currents remain approximately the same, even if the shading rate varies. However, under scenarios of low-shading rates, the current decreases sharply with an increase in voltage within the low-voltage region.

On the other hand, Figure 5 illustrates how to determine any point of the module characteristic. The module voltage (V_{mod_sh}) for a given current is the sum of the partially shaded cell voltage $\left(V_{cell\_sh}\right)$ and $\left(n_s - 1\right)$ times the irradiated (or unshaded) cell voltage $\left(V_{cell_{unsh}}\right)$, where n_s represents the total number of series-connected cells in a PV module (Quashning, 2005). To reconstruct the total module characteristic for the shaded case, we just need to calculate the module voltages point by point for different currents, selecting a range of currents from zero to the unshaded short-circuit current. This can be accomplished using the equation provided above.

$$V_{mod\_sh}(I) = V_{cell_{sh}}(I) + (n_s - 1)\ V_{cell_{unsh}}(I) \tag{9}$$

In the context of PV systems, it is often challenging to directly measure the current–voltage (I–V) characteristic of an individual unshaded solar cell integrated within a PV module. Instead, measurements are typically taken for the entire PV module, encompassing both shaded and unshaded cells, regardless of whether the module is fully illuminated (unshaded) or partially shaded. Therefore, Eq. (10), which relates to this measurement methodology, can be adapted to account for the voltages of both the shaded cell and the unshaded module, thereby enhancing the accuracy of our analysis.

$$V_{mod\_sh}(I) = V_{cell_{sh}}(I) + \left(\frac{n_s - 1}{n_s}\right) V_{mod_{unsh}}(I) \tag{10}$$

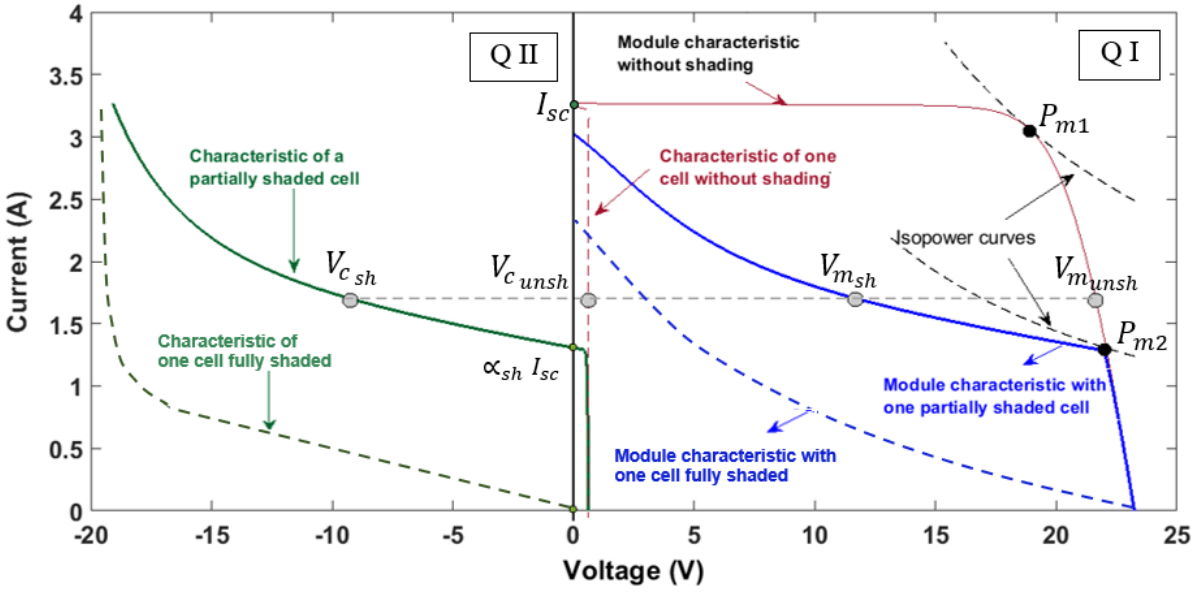

Figure 5. Construction of the PV module characteristic with one partially shaded cell. PV, photovoltaic.

Using Eq. (11) (provided below), we can determine the reverse voltage of the shaded cell. This can be achieved by subtracting the voltage of the unshaded module from that of the shaded one. This subtraction process allows us to isolate and quantify the voltage contribution of the shaded cell within the PV module, providing valuable insights into its performance.

$$V_{cell_{sh}}(I) = V_{mod_{sh}}(I) - \left(\frac{n_s - 1}{n_s}\right) V_{mod_{unsh}}(I) \tag{11}$$

It also should be noted that, as depicted in Figure 5, the partially shaded cell's reverse I–V curve starts at $(V, I) = (0, (1 - \propto_{sh}) I_{sc})$, where $\propto_{sh}$ represents the shading rate (ranging from 0 for a fully illuminated cell to 1 for a fully shaded cell) and I_{sc} is the short-circuit current of the unshaded cell. For a fully shaded cell, the starting point is (0, 0), which defines the dark I–V curve (the specific reverse I–V curve for a fully shaded cell). By fitting the latter curve, we can identify the parameters required for the models in the second quadrant (QII).

4.2. Method description

As described in the previous section using Eq. (11), the I–V characteristic of a reverse-biased cell within a PV module can be indirectly obtained without disassembling the module. This is achieved by simultaneously measuring the voltages of both the shaded and unshaded modules under identical weather conditions (irradiance (G) and temperature (T)). The subsequent sections and Figure 6's flowchart illustrate the measurement procedure using this proposed method.

- In the initial step of our procedure, it is necessary to remove the bypass diodes (BPDs) included in the junction box of the PV module. It is worth mentioning that commercial PV modules are equipped with BPDs to mitigate mismatch effects resulting from partial shading, hotspot heating, manufacturing variances, and other factors.
- In the second step, we measure the I–V curve of a fully illuminated (unshaded) PV module for voltage values ranging from 0 to the open-circuit voltage (V_{oc}). Simultaneously, under similar irradiance and temperature conditions, we measure the I–V characteristic of another identical PV module, similar to the previous one but with one cell fully shaded. Here, the shaded cell is covered by a piece of opaque material to ensure complete darkness. The voltage range for this measurement also spans from 0 to V_{oc}.
- In the third step, we utilise appropriate software or tools to fit the acquired I–V curve of a fully illuminated PV module using either the SDM or the DDM (as described by Eq. (1)). We then record the fitting parameters,

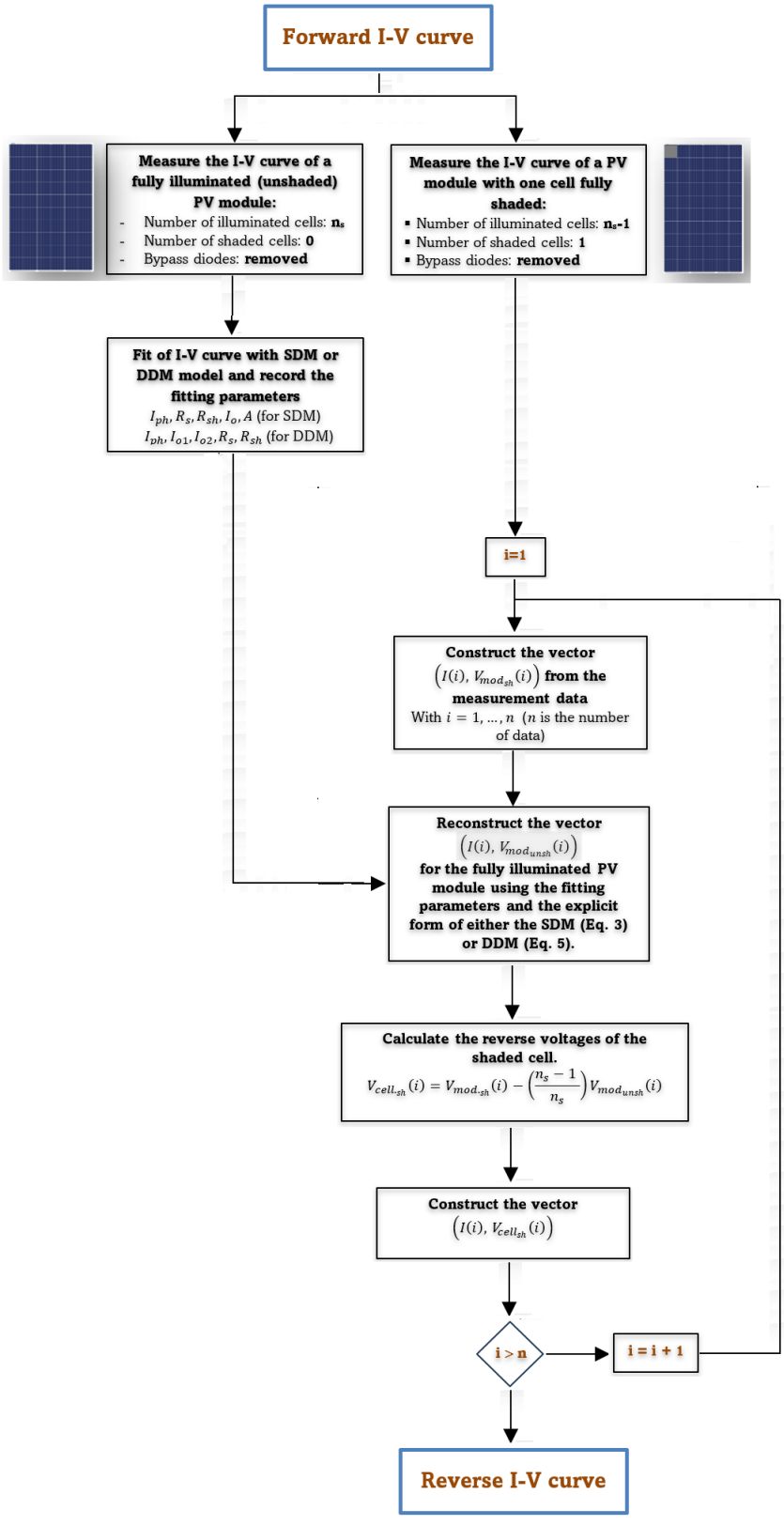

Figure 6. Flowchart describing the steps to obtain the I–V characteristic of a PV cell integrated into a module. DDM, double-diode model; PV, photovoltaic, SDM, single-diode model.

including the light-generated current (I_{ph}), the reverse saturation current (I_o), the ideality factor (A), the series resistance (R_s), and the shunt resistance (R_{sh}).

– In the fourth step, we construct the vector (I(i), $V_{mod_{sh}}(i)$) using the measurement data, where I(i) represents the measured current at index *i (i = 1*,2,3,…*n)* and $V_{sh}(i)$ represents the measured shading voltage at index *i*.
– In the fifth step, we use the fitting parameters to reconstruct the I–V curve for the fully illuminated module using the explicit form of either the SDM (Eq. (3)) or DDM (Eq. (5)). This generates the vector ($I(i)$, $V_{mod_{unsh}}(i)$), where I(i) is the measured current of the shaded module at index i, and $V_{mod_{unsh}}(i)$ is the calculated voltage using the chosen model's equation.
– In this final step, using Eq. (11), we extract the I–V characteristic curve representing the reverse-bias behaviour of the shaded cell. This process indirectly yields the desired information about the cell's performance under reverse-bias conditions. Finally, we can employ suitable software tools such as MATLAB, C++, or Origin to extract the fitting parameters associated with the Roger, Bishop, and Quashing models.

5. Experimental Validation of the Proposed Method

To confirm and assess the practical feasibility of the proposed method for measuring the reverse bias I–V curve of an individual PV cell within a PV module without disassembling it, outdoor measurements (i.e., under natural sunlight) were conducted on two identical commercial PV modules. Specifically, these are the Isofoton I-106 PV modules, each consisting of 72 monocrystalline silicon cells arranged in series and equipped with 3 BPDs. Their parameters are detailed in Table 1, as provided by the manufacturer under STCs.

5.1. Experimental setup and measurement equipment

As previously mentioned, the principle of measuring a reverse-biased cell's I–V characteristic is quite straightforward. Figure 7 illustrates the schematic of the experimental setup and measurement equipment required to perform this method. Both modules are exposed to the same normal insolation, with one cell completely covered in the shaded module. A current–voltage curve tracer (IVT-12-1000) swiftly switches between the modules via a tripolar switch to obtain their I–V curves almost simultaneously. To monitor climatic parameters, a Pt-100 sensor is attached to one module's backskin to measure cell temperature, while a pyranometer measures the incident global irradiance.

To further validate the proposed method, indoor measurements of the reverse bias I–V curve were conducted in the laboratory on an extra silicon solar cell identical to those used in the Isofoton I-106 PV module. This curve is obtained by connecting the cell to an external variable DC voltage source with opposite polarity. As a useful tool for characterising solar cells, the reverse bias I–V curve can be used to validate the proposed method.

5.2. Results and discussion

To evaluate the effectiveness of the proposed method described above, which can allow us to reproduce the I–V curve in the second quadrant (reverse bias I–V curve) and consequently determine the inverse parameters relative to the Roger, Bishop, and Quashning models, this section presents several cases involving outdoor measurements on a commercial PV module. Firstly, we recorded the I–V characteristics for the first quadrant (the forward bias)

Table 1. Manufacturer electrical parameters of the Isofoton I-106 PV module at STC (1,000 W/m²; 25°C)

Parameters	Value	Unit
Maximum power	106	W
Voltage at maximum power	34.80	V
Current at maximum power	3.05	A
Short-circuit current	3.27	A
Open circuit voltage	43.20	V
Diode saturation current	0.24	nA
Diode quality factor	1.011	–
Shunt resistance	3,000	Ω
Series resistance	1.01	Ω

PV, photovoltaic; STC, standard test conditions.

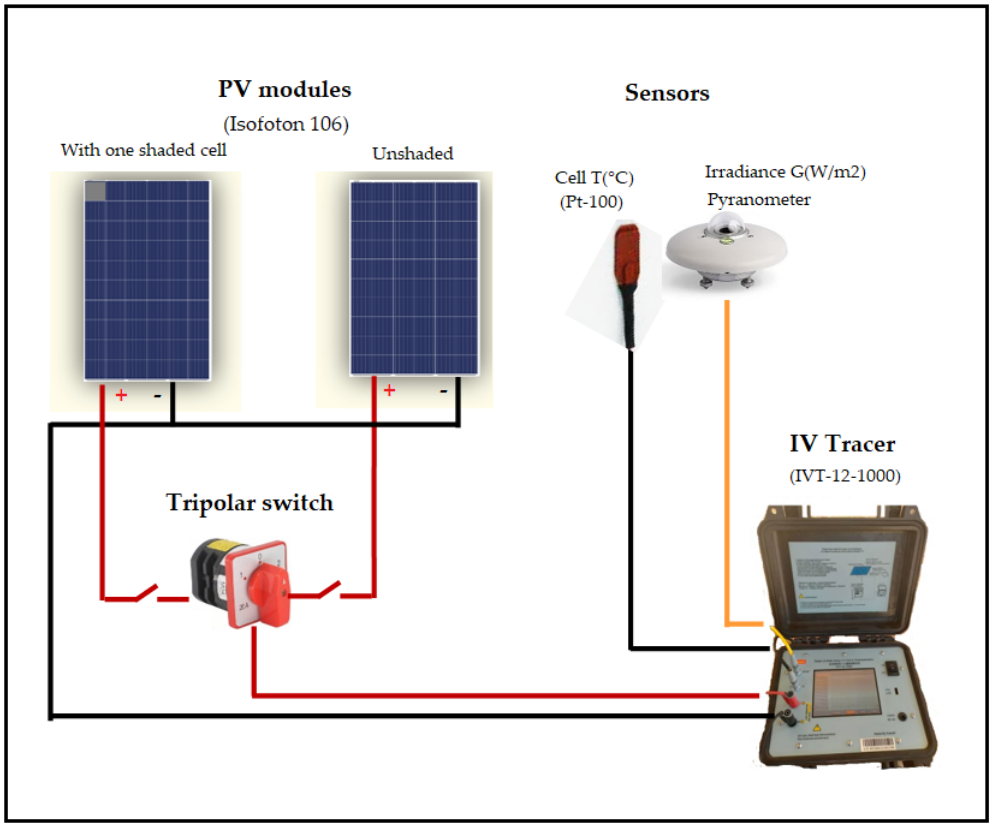

Figure 7. Diagram of the outdoor measurement system based on incident irradiance and cell temperature, and an I–V tracer. PV, photovoltaic.

I-V_1 and I-V_2o for the unshaded and shaded PV modules under three different conditions of solar irradiance and cell temperature: 665 W/m² at 39°C, 825 W/m² at 45°C, and 940 W/m² at 49°C, as shown in Figures 8a–8c. Next, we estimated the five parameters of the first quadrant only for the unshaded PV module under these specific weather conditions. Subsequently, we derived the parameters of a cell constituting this same module, as illustrated in Table 2.

Furthermore, we used Eq. (3) (provided below) and the cell parameters from Table 1 to obtain the I–V curve for a single cell within the unshaded PV module. Then, Eq. (11) was employed to determine the reverse voltage of the shaded cell. This involved subtracting the voltage of the unshaded module from $(n_s - 1)/n_s$ times the voltage of the shaded cell, where $n_s = 72$. The resulting I–V curves, generated for various irradiance and temperature conditions are depicted as 'IV4' (indicated by a dashed red line) in the second quadrants of Figures 8a–8c.

To experimentally validate our results, we overlaid the reverse bias I–V curve, which was measured in the laboratory for a separate PV cell, onto the second quadrants of Figures 9a–9c (indicated by a thick blue dotted line). The obtained results highlight that the IV curves obtained by the proposed method (indirect method) are well correlated and agree with the experimental I–V curve (direct method). In terms of the coefficient of determination *R*-square, the obtained values are close to 1. Also, the obtained values for the mean bias errors (MBEs) are almost negligible. It should be noted that, although variations in climatic parameters such as irradiance and temperature affect the measured I–V curves of the PV module in the first quadrant (shown in Figures 8a–8c for IV1 and IV2), this variability has almost a negligible impact on determining the characteristics of the PV cell in the second quadrant (the reverse-bias region).

After obtaining the reverse-bias I–V curves of the Isofoton PV cell, we used a nonlinear implicit function fitting tool to extract the model parameters. This process identified the fitting parameters related to the Rogers model (B_{rev}), the Bishop model (a, n, and V_{br}), and the Quashing model (a, n, and V_{br}). These parameters are detailed in Table 3, with their corresponding fitting curves displayed in Figures 9a–9c. Significantly, the extracted cell parameters for each model exhibit outstanding alignment between the fitting curves and the experimental data.

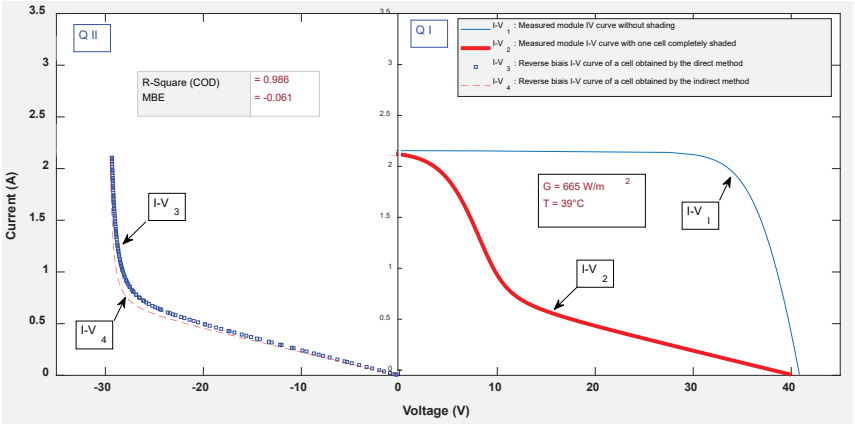

(a)

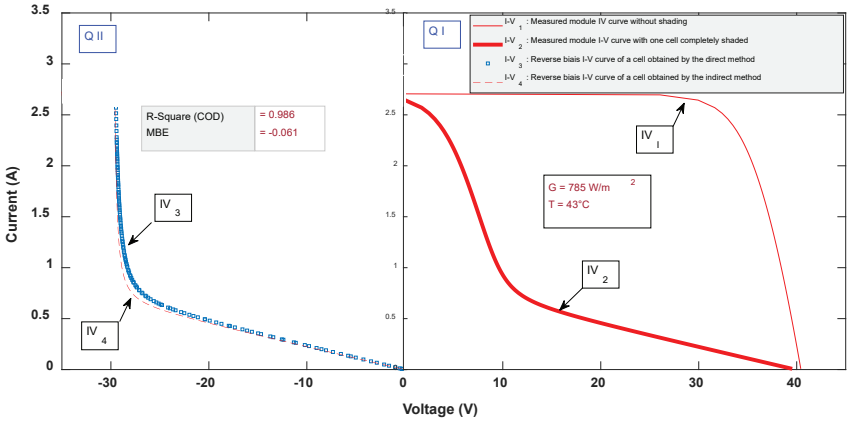

(b)

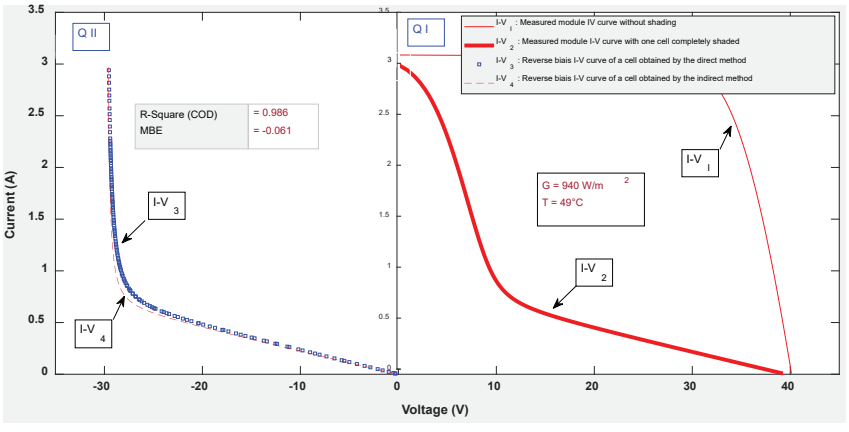

(c)

Figure 8. In quadrant II, the reverse-bias I–V curve (I–V3: thick blue dotted line) of a PV cell within an Isofoton I-106 PV module obtained using the proposed method (indirect method) is compared with the measured I–V curve (I–V4: dashed red line) of an identical but separate PV cell using the direct method. In quadrant I, the forward bias I–V curve (I–V1: thin red line) for a fully illuminated PV module and the I–V curve (I–V2: thick red line) of the PV module with one covered PV cell under various weather conditions (irradiance, G, and cell temperature, T) are shown for: (a) G = 665 W/m^2, T = 39°C, (b) G = 785 W/m^2, T = 43°C, and (c) G = 940 W/m^2, T = 49°C. PV, photovoltaic.

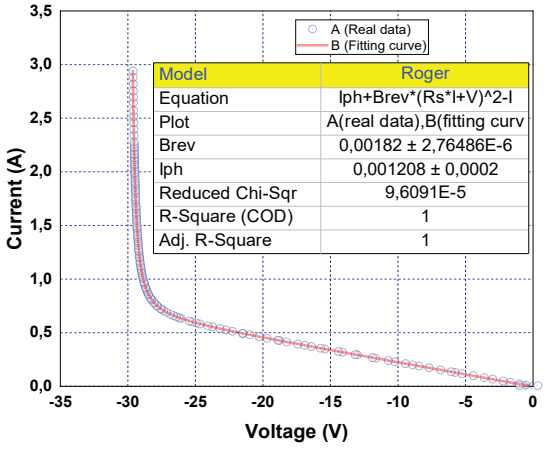

(a) Roger parameter (B_{rev})

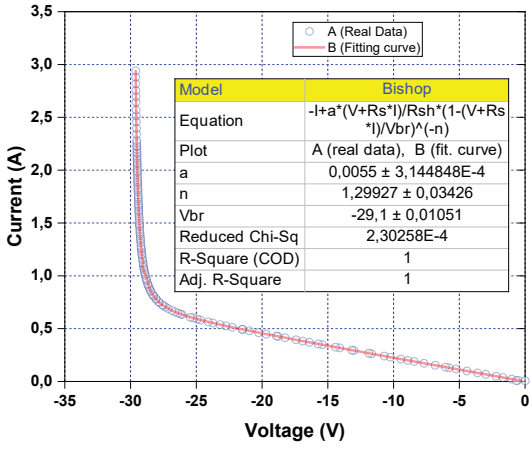

(b) Bishop parameters (a, n, V_{br})

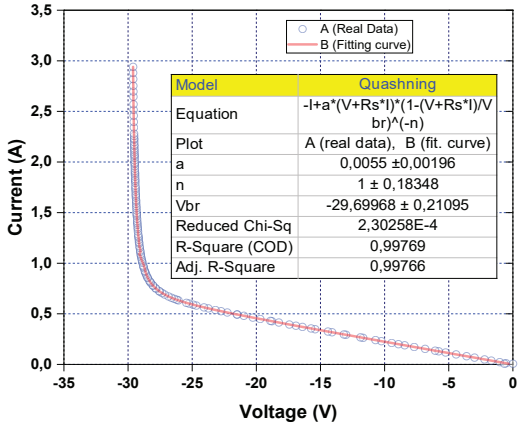

(c) Quashning parameters (a, n, V_{br})

Figure 9. Comparison of reverse-biased I–V curves obtained via proposed method and fitting curves using the Roger, Bishop, and Quashning models. a) Roger parameter (B_{rev}), b) Bishop parameters (a, n, V_{br}), c) Quashning parameters (a, n, V_{br}).

Table 2. Forward parameters extracted for the Isofoton 106 PV cell, related to the SDM model

Weather conditions		Forward parameters				
Irradiance	cell temperature	I_{ph}	I_o	R_s	R_{sh}	A
(W/m^2)	(°C)	(A)	(A)	(Ω)	(Ω)	–
665	39	2.175	1.895×10^{-9}	1.015	64.66	1.011
		±0.22%	±0.15%	±0.20%	±0.10%	±0.02%
825	45	2.698	4.334×10^{-9}	0.013	52.12	1.011
		±0.21%	±0.19%	±0.19%	±0.11%	±0.02%
940	49	3.075	1.895×10^{-9}	0.014	45.74	1.011
		±0.23%	±0.17%	±0.17%	±0.15%	±0.02%

PV, photovoltaic; SDM, single-diode model.

Table 3. Reverse parameters extracted for the Isofoton 106 PV cell, related to the Roger, Bishop, and Quashning models

Model	Reverse parameters			
	A	n	V_{br} (V)	B_{rev} (A/V^2)
Roger	–	–	–	0.00182
Bishop	0.0055	1.29927	−29.1	–
Quashning	0.0055	1	−29.27	–

PV, photovoltaic.

6. Conclusion

A novel method has been proposed to reproduce the reverse-biased I–V characteristics of individual PV cells within a module without disassembling the module from its encapsulant. The method's principle is quite straightforward: It involves conducting simultaneous outdoor measurements (under consistent weather conditions, irradiance, and temperature) of the forward-bias I–V curves using commercially available I–V tracers. The measurements are taken on two identical PV modules with a series configuration of the cells and in the absence of BPDs. One module is fully illuminated, while the other has only one fully shaded cell. From these two obtained forward-bias I–V curves, the reverse I–V curve can be easily extracted.

To validate the accuracy of the proposed method, comparisons were made between the I–V curves obtained using our method and those obtained directly in the laboratory. The results showed good agreement. Additionally, fitting the reverse-biased I–V curves allows us to extract the reverse parameters such as the breakdown voltage and certain correlation coefficients associated with the Roger, Bishop, and Quashing models.

In conclusion, the proposed method offers a nondestructive technique for characterising solar cells under reverse bias conditions. This innovative approach presents a promising solution for assessing the PV module performance and health without causing damage, potentially leading to significant cost savings.

References

Aktaş, A. and Kirçiçek, Y. (2021). Chapter 1 – Solar system characteristics, advantages, and disadvantages. In: *Solar Hybrid Systems-Design and Application*. 1st edition, 2021. Academic Press. pp. 1–24. doi: 10.1016/B978-0-323-88499-0.00001-X.

Babu, B. C., Gurjar, S. and Meher, A. (2015). Analysis of Photovoltaic (PV) Module During Partial Shading Based on Simplified Two-Diode Model. *International Journal of Emerging Electric Power Systems*, 16(1), pp. 15–21 doi: 10.1515/ijeeps-2014-0164.

Bastidas, JD., Franco, E., Petrone, G., Ramos-Paja, CA. and Spagnuolo, G. (2013). A Model of Photovoltaic Fields in Mismatching Conditions Featuring an

Improved Calculation Speed. *Electric Power Systems Research*, 96, pp. 81–90. doi: 10.1016/j.epsr.2012.10.020.

Batzelis, E. I., Anagnostou, G., Chakraborty, C. and Pal, B. C. (2020). Computation of the Lambert W Function in Photovoltaic Modeling. *Electrimacs*, 604, pp. 583–595.

Batzelis, E. I., Routsolias, I. A. and Papathanassiou, S. A. (2014). An Explicit PV String Model Based on the Lambert W Function and Simplified MPP Expressions for Operation Under Partial Shading. *IEEE Transactions on Sustainable Energy*, 5(1), pp. 301–312. doi: 10.1109/TSTE.2013.2282168

Bishop, J. W. (1988). Computer Simulation of the Effects of Electrical Mismatches in Photovoltaic Cell Interconnection Circuits. *Solar Cells*, 25, pp. 73–89. doi: 10.1016/0379-6787(88)90059-2

Ćalasan, M., Abdel, S. H. E. and Zobaa, A. F. (2020). On the Root Mean Square Error (RMSE) Calculation for Parameter Estimation Of Photovoltaic Models: A Novel Exact Analytical Solution Based on Lambert W Function. *Energy Conversion and Management*, 210, p. 112716. doi: 10.1016/j.enconman.2020.112716

Duong, M. Q., Sava, G. N., Ionescu, G., Necula, H., Leva, S. and Mussetta, M. (2017). Optimal bypass diode configuration for PV arrays under shading influence. In: *IEEE International Conference on Environment and Electrical Engineering*, 06-09 June 2017, Milan, Italy: IEEE. doi**:** 10.1109/EEEIC.2017.7977526.

Drif, M., Bahri, M. and Saigaa, D. (2021). A Novel Equivalent Circuit-Based Model for Photovoltaic Sources. *Optik – International Journal for Light and Electron Optics*, 242, p. 167046. doi: 10.1016/j.ijleo.2021.167046.

Gallardo-Saavedra, S. and Karlsson, B. (2018). Simulation, Validation and Analysis of Shading Effects on a PV System. *Solar Energy*, 170, pp. 828–839. doi: 10.1016/j.solener.2018.06.035

Gbadega Peter, A. and Saha, A. K. (2019). Electrical characteristics improvement of photovoltaic modules using two-diode model and its application under mismatch conditions. In: *Southern African Universities Power Engineering Conference*, 28–30 January 2019, Bloemfontein, South Africa: IEEE, pp. 328–333. doi: 10.1109/RoboMech.2019.8704846.

Häberlin, H. (2012). *Photovoltaics: System Design and Practice*, 1st ed. Wiley-Interscience Publication. Chichester, West Sussex, United Kingdom.

Hurkx, G. A. M., de Graaff, H. C., Kloosterman, W. J. and Knuvers, M. P. G. (1992). A New Analytical Diode Model Including Tunneling and Avalanche Breakdown. *IEEE Transactions on Electronic Devices*, 39(9), pp. 2090–2098. doi: 10.1109/16.155882.

Ishaque, K., Salam, Z. and Taheri, H. (2011). Simulation Modelling Practice and Theory Modeling and simulation of photovoltaic system during partial shading based on a two-diode model. *Simulation Modeling Practice and Theory*, 19(7), pp. 1613–1626.

Ishaque, K. and Salam, Z. (2013). A Review of Maximum Power Point Tracking Techniques of PV System for Uniform Insolation and Partial Shading Condition. *Renewable and Sustainable Energy Reviews*, 19, 475–488. doi: 10.1016/j.rser.2012.11.032.

Jain, A. and Kapoor, A. (2004). Exact Analytical Solutions of the Parameters of Real Solar Cells Using Lambert W-Function. *Solar Energy Materials and Solar Cells*, 81, pp. 269–277. doi: 10.1016/j.solmat.2003.11.018

Jain, A., Sharma, S. and Kapoor, A. (2006). Solar Cell Array Parameters Using Lambert W-Function. *Solar Energy Materials and Solar Cells*, 90(1), pp. 25–31. doi: 10.1016/j.solmat.2005.01.007

Kadri, R., Andrei, H., Gaubert, J. P., Ivanovici, T., Champenois, G. and Andrei, P. (2012). Modeling of the Photovoltaic Cell Circuit Parameters for Optimum Connection Model and Real-Time Emulator with Partial Shadow Conditions. *Energy*, 42(1), pp. 57–67. doi: 10.1016/j.energy.2011.10.018

Karatepe, E., Boztepe, M. and Colak, M. (2007). Development of a Suitable Model for Characterizing Photovoltaic Arrays with Shaded Solar Cells. *Solar Energy*, 81(8), pp. 977–992.

Kim, K. A., Xu, C., Jin, L. and Krein, P. T. (2013). Photovoltaic Hot-Spot Detection for Solar Panel Substrings Using AC Parameter Characterization. *IEEE Journal of Photovoltaics*, 3(4), pp. 1134–1341.

Kermadi, M., Chin, V. J., Mekhilef, S. and Salam, Z. (2020). A Fast and Accurate Generalized Analytical Approach for PV Arrays Modeling Under Partial Shading Conditions. *Solar Energy*, 208, pp. 753–765. doi: 10.1016/j.solener.2020.07.077

Kreft, W., Przenzak, E. and Filipowicz, M. (2021). Photovoltaic Chain Operation Analysis in Condition of Partial Shading for Systems with and Without Bypass Diodes. *Optik*, 247, 167840. doi: 10.1016/j.ijleo.2021.167840

Lun, S. X., Wang, S., Yang, G. H. and Guo, T. T. (2015). A New Explicit Double-Diode Modeling Method Based on Lambert W-Function for Photovoltaic

Arrays. *Solar Energy*, 116(2015), pp. 69–82. doi: 10.1016/j.solener.2015.03.043

Moreira, H. S., de Souza Silva, J. L., dos Reis, M. V. G., de Bastos Mesquita, D., de Paula, P. H. K. and Villalva, M. G. (2021). Experimental Comparative Study of Photovoltaic Models for Uniform and Partially Shading Conditions. *Renewable Energy*, 164, pp. 58–73. doi: 10.1016/j.renene.2020.08.086.

Nehme, B., Sirdi, N. K. M., Akiki, T., Naamane, A. and Zeghondy, B. (2021). Chapter 2 – Photovoltaic Panels Life Span Increase by Control. *Predictive Modelling for Energy Management and Power Systems Engineering*, 1st edition, Elsevier. pp. 27–62. doi:10.1016/B978-0-12-817772-3.00002-1.

Ortiz-Conde, A. and Sánchez, F. J. G. (2005). Extraction of Non-Ideal Junction Model Parameters from the Explicit Analytic Solutions of its I-V Characteristics. *Solid-State Electronics*, 49, pp. 465–472. doi: 10.1016/j.sse.2004.12.001

Paraskevadaki, E. V., Papathanassiou, S. A. and Member, S. (2011). Evaluation of MPP Voltage and Power of mc-Si PV Modules in Partial Shading Conditions. *IEEE Transactions on Energy Conversion*, 26(3), 923–932. doi: 10.1109/TEC.2011.2126021.

Patel, H. and Agarwal, V. (2008). MATLAB-Based Modeling to Study the Effects of Partial Shading on PV Array Characteristics. *IEEE Transactions On Energy Conversion*, 23(1), pp. 302–310. doi: 10.1109/TEC.2007.914308.

Peng, L., Sun, Y. and Meng, Z. (2013). An Improved Model of Photovolatic Cell Using Lambert W Function. *Applied Mechanics and Materials*, 370, pp. 1196–1200.

Petrone, G., Spagnuolo, G. and Vitelli, M. (2007). Analytical Model of Mismatched Photovoltaic Fields by Means of Lambert W-Function. *Solar Energy Materials and Solar Cells*, 91(18), pp. 1652–1657.

Petrone, G. and Ramos-Paja, C. (2011). Modeling of Photovoltaic Fields in Mismatched Conditions for Energy Yield Evaluations. *Electric Power Systems Research*, 81, pp. 1003–1013. doi: 10.1016/j.epsr.2010.12.008.,

Petrone, G., Ramos-Paja, C. A. and Spagnuolo, G. (2017). *Photovoltaic Sources Modeling*. John Wiley & Sons Ltd. Chichester, West Sussex, United Kingdom.

Picault, D., Raison, B., Bacha, S., de la Casa, J. and Aguilera, J. (2010). Forecasting Photovoltaic Array Power Production Subject to Mismatch Losses. *Solar Energy*, 84(7), pp. 1301–1309.

Quashning, V. (2005). *Understanding Renewable Energy*. Earth Scan: London, UK.

Quashning, V. and Hanitsch, R. (1996). Numerical Simulation of Current-Voltage Characteristics of Photovoltaic Systems with Shaded Solar Cells. *Solar Energy*, 56(6), pp. 513–520.

Ramabadran, R. (2009). MATLAB Based Modelling and Performance Study of Series Connected SPVA Under Partial Shaded Conditions. *Journal of Sustainable Development*, 2(3), pp. 85–94.

Rathee, R. (2013). Comparative Analysis to Study the Effects of Partial Shading on PV Array with LT-Spice and Matlab/Simulink Environment. *International Journal of Engineering Research and Technology (IJERT)*, 2(5), pp. 1505–1508.

Roibás-Millán, E., Cubero-Estalrrich, J. L., Gonzalez-Estrada, A., Jado-Puente, R., Sanabria-Pinzón, M., Alfonso-Corcuera, D., Álvarez, J. M., Cubas, J. and Pindado, S. (2020). Lambert W-Function Simplified Expressions for Photovoltaic Current-Voltage Modelling. In: *IEEE International Conference on Environment and Electrical Engineering*, 09–12 June 2020, Madrid, Spain: IEEE, pp. 1–6. doi: 10.1109/EEEIC/ICPSEurope49358.2020.9160734.

Roger, A. and Maguin, C. (1982). Photovoltaic Solar Panel Simulation Including Dynamical Thermal Effects. *Solar Energy*, 29(3), pp. 245–256. doi: 10.1016/0038-092X(82)90210-9.

Samer, S., Ahmed, B. M. and Shehab, A. (2012). A Matlab/Simulink-Based Photovoltaic Array Model Employing Simpowersystems Toolbox. *Journal of Energy and Power Engineering*, 6(12), pp. 1965–1975.

Subramanian, Y. and Darling, R. B. (2001). Compact Modeling of Avalanche Breakdown in pn-Junctions for Computer-aided ESD Design (CAD for ESD). In: *Proceedings International Conference on Modeling and Simulation of Microsystems*, 19-21 March, 2001, South Carolina, USA. Vol. (1). pp. 48–51.

Tripathy, M., Kumar, M. and Sadhu, P. K. (2017). Photovoltaic System using Lambert W Function-Based Technique. *Solar Energy*, 158, pp. 432–439. doi: 10.1016/j.solener.2017.10.007

Varshney, S. K., Khan, Z. A., Husain, M. A. and Tariq, A. (2016). A comparative study and investigation of different diode models incorporating the partial shading effects. In: *International Conference on Electrical, Electronics, and Optimization Techniques (ICEEOT)*, 03–05 March 2016, Chennai, India: IEEE, pp. 3145–3150. doi: 10.1109/ICEEOT.2016.7755281.

Villalva, M., Gazoli, J. and Filho, E. (2009). Comprehensive Approach to Modeling and Simulation of Photovoltaic Arrays. *IEEE Transactions on Power Electronics*, 24(5), pp. 1198–1208. doi: 10.1109/TPEL.2009.2013862.

Wang, Y. and Hsu, P. (2009). Analytical Modelling of Partial Shading and Different Orientation of Photovoltaic Modules. *IET Renewable Power Generation*, 4(3), pp. 272–282. doi: 10.1049/iet-rpg.2009.0157.

Wei, W., Ning, L. and Shaoyuan, L. (2012). A Real-time Modeling of Photovoltaic Array. *Chinese Journal of Chemical Engineering*, 20(6), pp. 1154–1160. doi: 10.1016/S1004-9541(12)60601-6.

Yin, O. W. and Babu, B. C. (2018). Simple and Easy Approach for Mathematical Analysis of Photovoltaic (PV) Module Under Normal and Partial Shading Conditions. *Optik – International Journal for Light and Electron Optics*, 169, pp. 48–61. doi: 10.1016/j.ijleo.2018.05.037.